Vibrational and Electronic Spectroscopy of a Donor−Acceptor Substituted Distyrylbenzene and Its Covalent Dimers

Weinan Leng,[†] Jason Grunden,[‡] Glenn P. Bartholomew,[§] Guillermo C. Bazan,[§] and Anne Myers Kelley*[,†]

School of Natural Sciences, University of California, Merced, P.O. Box 2039, Merced, California 95344, Department of Chemistry, University of California, Santa Barbara, Santa Barbara, California 93106-9510, and Department of Chemistry, Kansas State University, Manhattan, Kansas 66506

Received: June 22, 2004; In Final Form: September 1, 2004

Absorption spectra, resonance Raman spectra and depolarization ratios, fluorescence spectra and emission polarizations, and simulations of the resonance Raman excitation profiles and absorption spectra are reported for a donor−acceptor substituted distyrylbenzene (DADSB) and two covalent "dimers" formed by joining two DADSB chains at their center phenyl ring through a paracyclophane moiety. Semiempirical and density-functional theory calculations of the ground-state geometries and ZINDO calculations of the electronic excitations are also reported. Both the spectroscopic results and the electronic structure calculations agree that the electronic states of these "dimers" are not adequately described by excitonic coupling between the nominally degenerate electronic transitions localized on each DADSB moiety. The resonance Raman spectra of both dimers are essentially identical but show additional lines and intensity differences relative to the monomer. The excitation profiles of all three molecules exhibit interference effects between the Raman amplitudes for the first two strongly allowed electronic transitions. All three molecules exhibit Raman depolarization ratios of 1/3 throughout the lowest-energy absorption band, but the fluorescence of both dimers immobilized in polymer matrixes is considerably depolarized relative to that of the monomer. This suggests that the electronic excitation, initially delocalized over both conjugated chains of the dimers, may become localized on a single chain as geometric relaxation and solvent reorganization occur.

Introduction

Many naturally occurring supramolecular structures, as well as man-made molecular materials, consist of noncovalent aggregates of conjugated molecules. In such aggregates, the intermolecular interactions are often weak enough to be considered as perturbations on the properties of the isolated molecules, yet strong enough that these perturbations are far from negligible. In many of these systems, such as the light-harvesting antenna pigments involved in photosynthesis,[1,2] the thin films of conjugated polymers used in organic light-emitting diodes,[3−6] and the donor−acceptor substituted poled polymers for second-order nonlinear optical applications,[7−10] it is the optical properties of the aggregates that are of principal interest. The simplest models for the electronic spectroscopy of such aggregates assume that no electron transfer or exchange occurs between monomers, in which case the intermolecular interaction simply involves the charge distributions on the individual monomers. For strongly allowed electronic transitions, the dominant term is the coupling between transition dipole moments on the constituent monomers, which splits the initially degenerate electronic excitations on the monomers into a band of transitions whose energies and oscillator strengths depend on the positions and relative orientations of the interacting molecules.[11−13]

There are some systems, such as the special pair in photosynthesis, in which the aggregates have a well-defined geometry. Many aggregates, however, contain a large number of randomly or semi-randomly positioned monomers encompassing a wide variety of different local interaction geometries. This heterogeneity presents a challenge for understanding the details of the intermolecular interactions or for predicting the optical properties of the aggregate. Many workers have therefore focused on simpler systems in which a small number of chromophores, often only two, are arranged in a well-defined geometry. Although noncovalent interactions sometimes provide dimers or even larger aggregates that appear to have a well-defined composition and geometry,[14−16] connecting the monomers through a covalent but electronically nonconjugated linkage is a more general and more certain way to force a single stoichiometry and spatial arrangement.

One convenient way to generate covalent dimers of monomers containing phenyl groups is to attach them through a paracyclophane linkage. The Bazan group, in particular, has synthesized and examined a number of such dimers based on stilbene, distyrylbenzene, and longer members of this series.[17−21] The original covalent dimers of nonpolar monomers were intended as model systems for the intermolecular interactions in para-(phenylene vinylene) and its substituted analogues used as organic LEDs. More recently, these studies have been extended to electron donor−acceptor substituted stilbenes and distyrylbenzenes.[22−25] These are interesting systems for addressing questions of through-space versus through-bond charge transfer and can be considered as model systems for the "push−pull" conjugated molecules useful as organic second-order nonlinear optical materials.

This paper describes spectroscopic and computational studies on a donor−acceptor substituted distyrylbenzene monomer and

* To whom correspondence should be addressed.
[†] University of California, Merced.
[‡] Kansas State University.
[§] University of California, Santa Barbara.

10.1021/jp047280f CCC: $27.50
Published on Web 10/27/2004

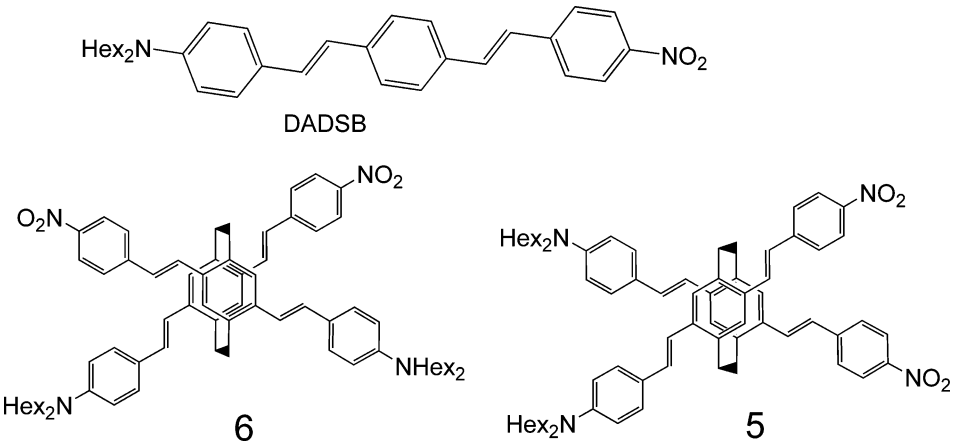

Figure 1. Monomer and two dimers studied in this work.

two of its paracyclophane-linked dimers that differ only in the relative orientation of the two monomers (Figure 1). The synthesis of these molecules and their absorption and fluorescence spectra in solution have already been reported,[24] as have their dipole moments and first hyperpolarizabilities.[25] Here we report and analyze their resonance Raman spectra and excitation profiles in solution and their fluorescence spectra and anisotropies in polymer films and present electronic structure calculations on both the ground-state geometry and the electronic excitations.

Experimental Methods

The synthesis and characterization of DADSB, **5**, and **6** have been described elsewhere.[24,25]

Absorption spectra were measured on a Hitachi U-3010 UV/vis spectrophotometer in 1 mm path length cells. Molar absorptivities were determined for DADSB, **5**, and **6** in CH_2Cl_2 by measuring spectra of carefully weighed samples. Absorptivities in $CHCl_3$ were determined by recording spectra of equal dilutions of CH_2Cl_2 stock solutions into CH_2Cl_2 and $CHCl_3$. These absorptivities were then used to determine the concentrations of the samples used for Raman spectroscopy.

Resonance Raman spectra of DADSB, **5**, and **6** were obtained in both CH_2Cl_2 and $CHCl_3$ solution at concentrations ranging from 0.03 to 0.6 mM. Two different excitation, sampling, and detection systems were employed. Spectra in CH_2Cl_2 were obtained on a 0.6-m Spex 1877E triple spectrograph utilizing reflective collection optics, a 1200 g/mm grating blazed at 500 nm in the spectrograph stage, and a liquid nitrogen cooled CCD detector. Samples of ~3 mL volume were contained in a spinning cell, illuminated with 1−20 mW of laser power focused with a 10 cm f.l. lens, and the Raman scattering collected in a ~135° backscattering geometry. Excitation wavelengths of 458, 488, and 514 nm were provided by a Lexel argon-ion laser, and excitation at 543 nm was obtained from a green He−Ne laser. Spectra in $CHCl_3$ were obtained on a 0.64-m Jobin-Yvon T64000 triple spectrograph with microprobe sampling (10× objective), either a 1200 g/mm grating blazed at 750 nm or an 1800 g/mm grating blazed at 500 nm in the spectrograph stage, and a UV coated, back-illuminated, liquid-nitrogen-cooled CCD detector. Samples of ~10 mL volume were circulated with a peristaltic pump through a 1 mm path length liquid flow cell, and Raman scattering was collected in a confocal 180° backscattering geometry. Excitation was provided by a Coherent Innova 90C argon-ion laser (363 nm and 458−514.5 nm), an argon ion-pumped Coherent 599 dye laser (563 nm), and a Spectra-Physics Tsunami Ti:sapphire laser producing 1−2 ps pulses at 82 MHz, frequency doubled to 400−450 nm. Laser powers at the sample were 1−10 mW for argon or dye laser excitation and no greater than 1 mW for Ti:sapphire excitation. In both instruments, the scattering was collected at 90° to the incident laser polarization direction and the scattered polarization was randomized by passage through a polarization scrambler placed before the spectrometer entrance slit. The intensities measured therefore correspond to the differential Raman cross section, $(d\sigma/d\Omega)_{||+\perp}$. For the Raman polarization measurements, the laser polarization was purified by passage through a Glan-Taylor prism, and a rotatable film polarizer was placed in the scattered beam path before the polarization scrambler.

Spectral resolution was 4−7 cm^{-1} depending on wavelength. Spectra were calibrated in Raman shift by reference to Raman lines of the solvent. Intensities were corrected for the spectral response of the spectrograph and detector by collecting spectra of a tungsten−halogen standard lamp as described elsewhere.[26] Intensities were corrected for reabsorption of the scattered light by using the algorithm derived in ref 27 for the experiments in CH_2Cl_2, where the samples were optically thick, and using a variation of the algorithm presented in ref 28 for the experiments in $CHCl_3$, which were performed at lower concentrations. Integrated peak areas were determined by fitting regions of the spectrum to sums of mixed Gaussian−Lorentzian peaks (Grams32) after subtraction of a low-order polynomial to remove underlying fluorescence. The absolute differential resonance Raman cross sections were determined by measuring the integrated areas of the chromophore Raman bands relative to that of the 702 cm^{-1} line of the CH_2Cl_2 solvent[29] or the 667 cm^{-1} line of the $CHCl_3$ solvent.[30] The A-term fitting parameters for $CHCl_3$, which refer to total Raman cross section, were converted to differential cross section using[26]

$$\left(\frac{d\sigma}{d\Omega}\right)_{||+\perp} = \left(\frac{3}{8\pi}\right)\left(\frac{1+\rho}{1+2\rho}\right)\sigma_T \qquad (1)$$

with $\rho = 0.02$ for the 667 cm^{-1} line of $CHCl_3$.

Resonance Raman depolarization ratios were measured for **5** and **6** in CH_2Cl_2 at 424, 458, and 514.5 nm excitation and in $CHCl_3$ at 563 nm. The incident laser polarization was purified by passage through a Glan-Taylor prism and the Raman scattering was detected through a sheet polarizer (Oriel) placed before the polarization scrambler. The detected polarization was alternated several times and the spectra at each polarization were summed. In the T64000 system, where the scattered light passes through a beam splitter at 45° before its polarization is scrambled, the intensities were corrected for the polarization dependence of the collection efficiency by collecting "parallel"

and "perpendicular" spectra of an unpolarized source (a tungsten−halogen lamp scattered off a $BaSO_4$ plate).

For the fluorescence measurements, samples in polystyrene (PS; Aldrich, MW 760−770) and poly(methyl methacrylate) (PMMA; Aldrich, MW 120,000) films were prepared as described previously[31] at chromophore concentrations of 10^{-5} to 10^{-6} by mass. Fluorescence spectra were obtained on a home-built fluorometer. The excitation source was a 150 W Xe−Hg lamp followed by an Oriel 0.125-m double monochromator. The detection system was a 0.65-m ISA spectrograph and a liquid nitrogen cooled Princeton Instruments CCD. The films were optically thin, and excitation and detection were nearly collinear. For anisotropy measurements, the excitation light was linearly polarized with one Polaroid sheet and parallel or perpendicularly polarized emission was selected with a second sheet, and a polarization scrambler was placed before the spectrograph entrance slit. All experiments were performed at ambient temperature. Fluorescence spectra have not been corrected for instrument response.

Computational Methods

Energy minimizations, normal mode calculations, and electronic structure calculations were carried out using the Gaussian 98 suite of programs[32] running under Windows. The hexyl groups were replaced by methyl groups. Ground-state geometries were calculated for all three molecules with the AM1 and PM3 semiempirical Hamiltonians as well as density functional theory with the B3LYP hybrid density functional and two basis sets, STO-3G and 6-31G. Ground-state vibrational normal mode calculations were carried out for DADSB only using density functional theory with the 6-311G** basis set. Molden 3.6 was used to animate and visualize the normal modes.[33] Calculations of the electronic spectra were carried out using the ZINDO semiempirical method. The excited states were calculated using configuration interaction among all singly excited configurations formed from all 134 molecular orbitals for DADSB and from the 31 highest occupied and 50 lowest virtual orbitals for dimers **5** and **6**. Only the six (for DADSB) or 10 (for **5** and **6**) lowest electronic transitions were calculated.

The absorption and resonance Raman spectra were simulated via the time-domain wave packet method modified to consider contributions to the resonance enhancement from two different electronic states.[34,35] Each Raman-active mode was treated as a harmonic oscillator characterized by its frequency and a displacement Δ, in dimensionless normal coordinates, between the potential minima in the ground state and a given excited state. Changes in vibrational frequency upon excitation, mixing of the normal modes in the excited state (Duschinsky rotation), and coordinate dependence of the electronic transition moment were not considered. The electronic line width was partitioned into inhomogeneous broadening, modeled as a static Gaussian distribution of electronic zero−zero energies, and homogeneous broadening, described by coupling of the electronic transition to an overdamped Brownian oscillator representing the solvent degrees of freedom. Complete correlation between the shifts of both electronic transitions within the inhomogeneous distribution was assumed[36] (but see also ref 34). The parameters were adjusted to obtain the best simultaneous fit to the absorption spectrum and the absolute resonance Raman cross sections at all measured wavelengths. The second absorption band (near 370 nm) may be composed of more than one electronic transition, and the longest-wavelength band probably also contains more than one transition, at least in the dimers (vide infra). However, the wavelength-dependent Raman intensities give direct evidence for only two contributing transitions.

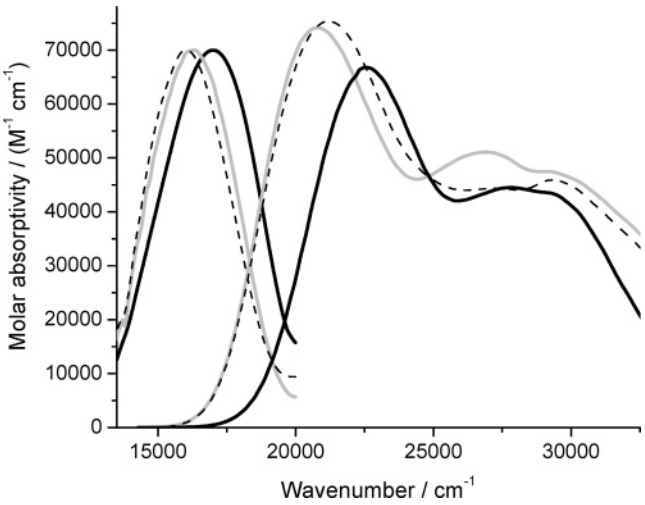

Figure 2. Absorption spectra in CH_2Cl_2 (units on *y* axis) and fluorescence spectra in PMMA films (arbitrarily scaled) for DADSB (solid black), dimer **5** (solid gray), and dimer **6** (dashed). Fluorescence excitation wavelengths are 450 nm for DADSB and 475 nm for the dimers.

Results

Absorption Spectra. Figure 2 shows the linear absorption spectra of DADSB, **5**, and **6** in CH_2Cl_2. The monomer has a strong transition at about 22 500 cm^{-1} and a broader band, which may encompass more than one transition, at 26 000 to 30 000 cm^{-1}. The two dimers, **5** and **6**, have very similar spectra with the low-energy band shifted to the red by 1000−2000 cm^{-1} and some changes in the shape of the higher-energy band(s). Notice that the integrated molar absorptivity of the dimers is only slightly greater than that of the monomer even though the dimers contain two DADSB chromophores.

Fluorescence Spectra and Anisotropies. The fluorescence spectra in fluid solution were reported in ref 24. To gain further insight into the nature of the absorbing and emitting states, we measured fluorescence spectra and anisotropies of the chromophores immobilized in PMMA and PS matrixes. Here the chromophores are randomly oriented but have little ability to rotate between the light absorption and emission steps. The fluorescence spectra in PMMA, excited near the absorption maxima, are shown in Figure 2. All three molecules have very similar spectra, with the dimer spectra slightly red-shifted relative to that of the monomer. The fluorescence spectra in hexanes, which show some vibronic structure, are also quite similar for all three molecules.[24] The emission maxima in PMMA show a significant dependence on excitation wavelength as shown in Figure 3. For the monomer, excitation at shorter wavelengths leads to emission at shorter wavelengths with excitation in the 400−500 nm range. This behavior is consistent with the existence of an inhomogeneous distribution of absorbers that differ in the local polarity or refractive index of the medium and/or the planarity of the chromophore.[37] Excitation at different wavelengths photoselects different subsets of the inhomogeneous population which do not interconvert during the fluorescence lifetime, so redder excitation produces redder emission. At even shorter excitation wavelengths (375−350 nm), the higher-energy band starts to contribute significantly to the absorption and the contribution of redder-emitting molecules increases again. The dimers show the same trend for excitation within the low-energy absorption band at 425−550 nm, but at shorter excitation wavelengths (400−350 nm), where the second transition should start to contribute significantly, the emission further blue-shifts.

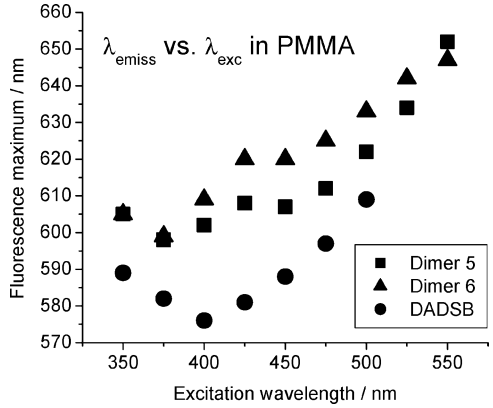

Figure 3. Dependence of fluorescence maximum on excitation wavelength for DADSB and dimers **5** and **6** in PMMA films at room temperature.

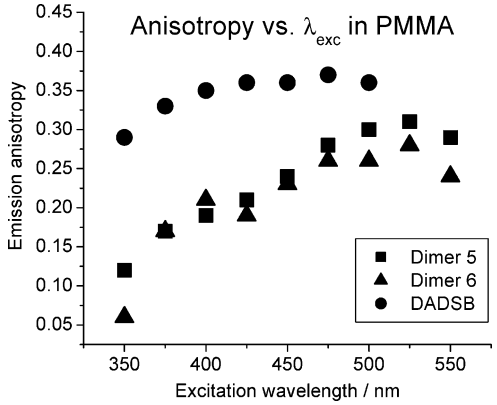

Figure 4. Fluorescence anisotropy as a function of excitation wavelength for DADSB and dimers **5** and **6** in PMMA at room temperature.

Figure 4 plots the fluorescence anisotropy, $r = (I_{||} - I_{\perp})/(I_{||} + 2I_{\perp})$, as a function of excitation wavelength in PMMA. The anisotropies at a given excitation wavelength are only weakly dependent on emission wavelength and are nearly constant over the region where there is significant emission. For the monomer, excitation within the main absorption band (400−500 nm) results in a fluorescence anisotropy only slightly below the value of $r = 0.4$ expected for a single electronic transition of a randomly oriented sample unable to rotate during the fluorescence lifetime. The slight deviation from 0.4 may indicate a small degree of rotational freedom within the polymer matrix. Both dimers show considerably lower anisotropies even when excited within the main absorption band (450−550 nm). Similar anisotropy data were obtained in PS films, although in general the anisotropies were slightly lower in PS.

Resonance Raman Spectra and Depolarization Ratios. Figure 5 displays the resonance Raman spectra of all three molecules in CH_2Cl_2 at an excitation wavelength of 458 nm. The dimer spectra are virtually identical to each other and differ from the monomer spectrum mainly in the "fingerprint" region around 1150−1300 cm^{-1}. The frequencies and relative intensities are nearly independent of excitation wavelength within the main absorption band (above ∼430 nm for the monomer and above ∼450 nm for the dimers). Figure 6 shows the Raman polarization data of the dimers with excitation at 458 nm. For all Raman lines, the depolarization ratio $\rho = I_{\perp}/I_{||}$ is nearly identical to 0.33, the value expected for resonance with a single allowed electronic transition. Essentially identical results were obtained using excitation at 514.5 nm and on the red edge of the absorption at 563 nm, but a slightly higher value of $\rho = 0.4$ was obtained for both **5** and **6** when excited at 424 nm, where the higher-energy band is starting to contribute to the absorption.

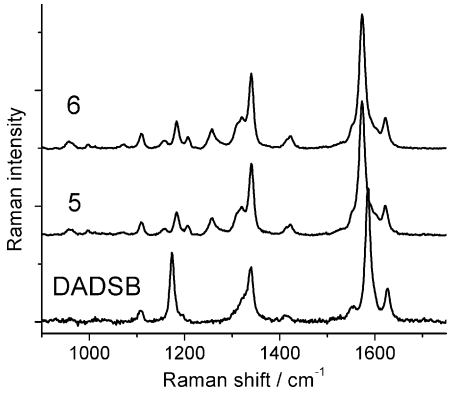

Figure 5. Resonance Raman spectra of DADSB and dimers **5** and **6** in CH_2Cl_2 solution at 458 nm excitation. Intensity scale is arbitrary. Fluorescence backgrounds have been subtracted and dimer spectra are offset vertically for clarity.

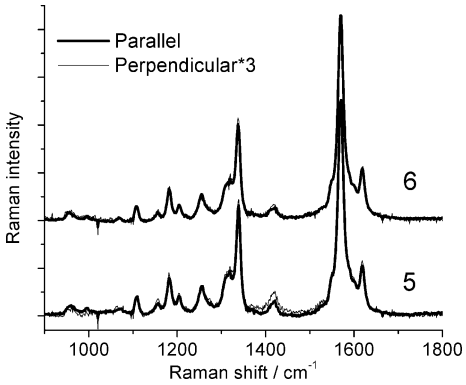

Figure 6. Polarized resonance Raman spectra of dimers **5** and **6** in CH_2Cl_2 at 458 nm excitation. Fluorescence backgrounds have been subtracted from all spectra and the perpendicular spectra multiplied by a factor of 3. Relative scaling and vertical offset of the **5** and **6** spectra is arbitrary. The parallel and perpendicular*3 spectra are nearly indistinguishable.

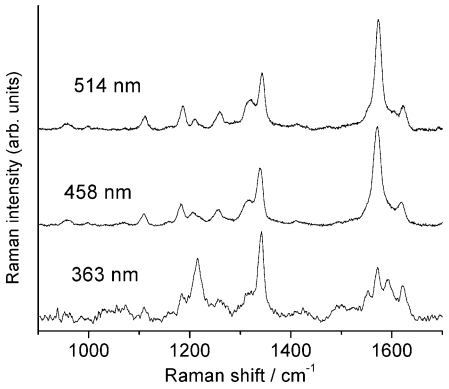

Figure 7. Resonance Raman spectra of dimer **5** in $CHCl_3$ at three excitation wavelengths. Vertical scales and vertical offsets are arbitrary.

Figure 7 compares the Raman spectra of dimer **5** obtained with excitation on the red side of the first absorption band, on the blue side of that band, and within the second absorption band. The spectral patterns are nearly the same throughout the main absorption band, but clearly become very different when exciting into the higher-energy band. This indicates that the geometry changes induced by excitation into the higher-energy and lower-energy bands are quite different, and localized on different parts of the molecule.

TABLE 1: Calculated Geometries for DADSB and Dimers 5 and 6 from Different Methods, and Calculated (ZINDO) Electronic Transition Wavelengths, Oscillator Strengths, and Polarizations at Each Geometry

method[a]	AM1			PM3			B3LYP/STO-3G			B3LYP/6-31G		
	state[b]	nm	*f*, pol.[c]	state[b]	nm	*f*, pol.[c]	state[b]	nm	*f*, pol.[c]	state[b]	nm	*f*, pol.[c]
DADSB	3	409	1.95, x	3	403	1.83, x	3	457	1.14, x	1	444	1.68, x
	4	345	0.09, xy	4	342	0.13, x	4	368	0.88, x	2	366	0.40, x
geom[d]	spiral twisted 0°/45°/90°, $r_{Ce=Ce}$=1.34, r_{NO}=1.20, $r_{Ce-Cphen}$=1.45, μ=3.8 D			planar, $r_{Ce=Ce}$=1.34, r_{NO}=1.23, $r_{Ce-Cphen}$=1.45			planar, $r_{Ce=Ce}$=1.36, r_{NO}=1.32, $r_{Ce-Cphen}$=1.49, μ=7.7 D			planar, $r_{Ce=Ce}$=1.36, r_{NO}=1.27, $r_{Ce-Cphen}$=1.46, μ=13.1 D		
dimer **6**	4	438	0.89, x	4	443	1.12, x	5	511	0.12, y	3	486	0.16, y
	7	406	0.19, y	5	423	0.15, y	6	490	1.45, x	6	459	2.11, x
	8	390	0.92, x	8	401	0.96, x	7	463	0.15, y	7	439	0.16, y
	9	381	0.20, x				10	391	0.39, x	10	377	0.31, x
geom[d]	rings twisted ~45°, slightly bent; $r_{Ce=Ce}$=1.34, r_{NO}=1.20, $r_{Ce-Cphen}$=1.45, μ=3.3 D			one unit planar, other NO_2 ring twisted ~45°; $r_{Ce=Ce}$=1.34, r_{NO}=1.22, $r_{Ce-Cphen}$=1.45−1.46			near planar, slightly bent; $r_{Ce=Ce}$=1.36, r_{NO}=1.32, $r_{Ce-Cphen}$=1.49, μ=7.1 D			NO_2 rings twisted 12°; $r_{Ce=Ce}$=1.36, r_{NO}=1.27, $r_{Ce-Cphen}$=1.46, μ=11.8 D		
dimer **5**	4	437	0.95, x	7	371	0.36, x	5	515	0.13, y	3	494	0.19, y
	7	410	0.22, y	8	337	0.78, y	6	479	1.60, x	6	456	2.39, x
	8	389	1.16, x	9	331	0.15, y	7	463	0.13, y	7	441	0.16, y
				10	328	0.23, z	10	387	0.42, x	10	366	0.23, x
geom[d]	NO_2 rings planar, $Nhex_2$ rings twisted ~30°; $r_{Ce=Ce}$=1.34, r_{NO}=1.20, $r_{Ce-Cphen}$=1.45, μ=6.1 D			near planar, bent ~120°; $r_{Ce=Ce}$=1.34, r_{NO}=1.22, $r_{Ce-Cphen}$=1.46			near planar, slightly bent; $r_{Ce=Ce}$=1.36, r_{NO}=1.32, $r_{Ce-Cphen}$=1.48−1.49, μ=13.7 D			NO_2 and $Nhex_2$ rings twisted <10°; $r_{Ce=Ce}$=1.36, r_{NO}=1.27, $r_{Ce-Cphen}$=1.46, μ=23.4 D		

[a] Ground-state geometry was minimized using each of the indicated methods. ZINDO calculations of the electronic transitions were then carried out at each geometry. [b] States are labeled in order from lowest to highest energy. States not listed have low (<0.1) oscillator strengths. [c] Oscillator strength *f* and dominant polarization of transition dipole. The molecule-fixed coordinate system is different for different geometries, so only the relative polarizations of different transitions calculated at the same geometry are relevant. [d] "Planar" or "twisted" refers to torsional angles between neighboring phenyl and ethylenic groups on a single chain; "bent" refers to bending of the two dimer chains perpendicular to the local plane of the phenyl groups. Ce = ethylenic carbon, Cphen = phenyl carbon. Calculated ground-state dipole moments are given for AM1 and DFT methods.

Electronic Structure and Normal Mode Calculations. Ground-state geometries of DADSB, **5**, and **6** were calculated with two semiempirical methods as well as density-functional theory with two different basis sets. The geometries obtained from the different methods varied considerably and are summarized in Table 1. The ZINDO semiempirical method was then used to calculate the energies and oscillator strengths for the low-energy electronic transitions of each chromophore starting from each of the calculated geometries. Table 1 summarizes the wavelength, oscillator strength, and polarization of each of the significantly allowed electronic transitions.

We do not have crystal structures of any of these molecules with which to compare the calculated geometries, and in any case, the solution phase structures might be quite different from the crystal structures particularly with regard to torsional angles. The low but nonvanishing intensity in the ethylenic hydrogen out-of-plane wagging mode near 960 cm^{-1} suggests that the average structure is slightly but not severely nonplanar.[38−40] For the monomer, the AM1 method finds a energy minimum at a significantly twisted geometry, whereas the PM3 and DFT geometries are essentially planar. This is consistent with our observations for other large conjugated molecules that DFT tends to produce much more planar geometries than AM1. Similarly, for both dimers, the AM1 geometry is considerably twisted, whereas the DFT geometries are nearly planar or only slightly twisted. The PM3 dimer geometries are quite odd; **6** has the paracyclophane and $Nhex_2$-substituted phenyl rings nearly coplanar and the NO_2-substituted ring twisted by about 45°, whereas in **5** there is almost no twisting of the phenyl groups but the entire distyrylbenzene unit is bent in a "butterfly" shape about 120° out of plane. Corresponding bond lengths are almost the same in the monomer and the dimers for a given computational method; the CC bond lengths do not vary greatly among different methods, but the NO bond lengths are much greater in the DFT methods than in the semiempirical ones. A calculation on DADSB only was also carried out using DFT with the 6-311G** basis, which includes diffuse functions. This basis yielded considerably shorter NO bonds (1.23 Å) and a slightly reduced dipole moment (12.0 D).

The electronic spectra calculated at the different ground-state geometries also vary considerably. The experimental absorption maxima for the longest-wavelength transition (in CH_2Cl_2) are 444 nm for DADSB, 481 nm for **5**, and 471 nm for **6**. The experimental oscillator strengths for this band, estimated by fitting the absorption spectra to sums of several Gaussians, are 1.26 for DADSB and 1.32 for the two dimers. Of the four methods, ZINDO with the B3LYP/STO-3G geometry does the best job of reproducing the experimental spectra. The calculations agree with the experimental result that the oscillator strength of the dimers is much less than twice that of the monomer, even if we sum the several calculated transitions of the dimers that are close in energy. For both dimers, and for the monomer at all geometries except the DFT/6-31G, the lowest two or more electronic transitions are essentially optically forbidden. The experimental spectra, on the other hand, give little evidence that the strongly absorbing state is not the lowest-energy one; all three molecules show only a small Stokes shift between absorption and emission in hexane, and the somewhat different vibronic structures of the absorption and emission spectra,[25] at least in DADSB, may be attributable to changes in vibrational frequencies between the ground and excited states.[41] We do not have the fluorescence lifetime and quantum yield data needed to evaluate whether the absorbing and emitting states have significantly different transition moments.

The experimental dipole moments for DADSB, **5**, and **6** are 7, 13.8, and 7 D, respectively.[25] These are very close to the values calculated from DFT with the STO-3G basis set, whereas AM1 greatly underestimates the dipole moments and DFT/6-31G greatly overestimates them.

TABLE 2: Experimental Frequencies and Tentative Normal Mode Descriptions for Resonance Raman Active Vibrations of DADSB, 5, and 6

DADSB freq./ cm^{-1}	DADSB RR intensity[a]	DADSB calc.[b] freq./ cm^{-1}	dimer **5** freq. $/cm^{-1}$	dimer **6** freq. $/cm^{-1}$	mode description[c]
601	w	608	604	604	N-hexyl$_2$ scissors and ring elongation (6a)
962	w	985, 993	961	959	C_e-H out-of-plane wags
1011	vw	1018, 1025, 1026	998	998	trigonal phenyl defs. (18a)
1110	m	1121	1109	1111	C−NO_2 stretch
			1158	1159	paracyclophane
1176	s	1206, 1211, 1220	1187	1185	ring CH rocks (9a)
			1208	1209	paracyclophane
			1259	1259	paracyclophane
1304	vw	1300, 1310	1309	1310	C_e-ϕ str.
1326	s	1353, 1354	1320	1321	C_e-H in-plane rocks
1342	s	1367	1342	1342	sym. NO_2 str.
1413	w	1389	1415	1416	C−N_{amino} str.
1552, 1561	m, w	1576, 1586	1554	1554	ring stretches (19a)
1588	vs	1679, 1680	1574	1575	C_e=C_e stretches
			1594	1595	center ring stretch (8a)
1605	vw	1638	1606	1607	A ring stretch (8a)
1630	m	1656	1624	1625	D ring stretch (8a)

[a] Qualitative intensity when excited within the longest-wavelength absorption band. [b] Density functional theory, B3LYP/6-311G**. [c] Notation for ring modes in parentheses is that of refs 43 and 44.

Ground-state vibrational frequencies and normal modes were calculated for DADSB using density functional theory with the 6-311G** basis set. Although the more primitive STO-3G basis gave more accurate ground-state dipole moments and perhaps better geometries, the 6-311G** vibrational frequencies were in much better agreement with the experiment. The calculated normal modes, along with comparison of the spectra of DADSB and its dimers and spectra and assignments for related molecules,[21,23,42] were used to make tentative assignments for the vibrations observed in the resonance Raman spectra. These are summarized in Table 2. The dimer bands near 1158, 1208, and 1259 cm^{-1}, not observed in the parent monomer, are assigned as partially or largely paracyclophane ring modes. The frequency shift and intensity redistribution of the 1176 cm^{-1} monomer mode in the dimers probably reflects changes in the ground-state normal mode descriptions, although changes in the excited-state geometries may also contribute. The assignments of the lines in the 1570−1630 cm^{-1} region are not clear-cut but almost certainly involve some combination of the ethylenic C=C stretches and "quinoidal" stretches of the phenyl groups (ring mode 8a, in-phase stretching of the two unsubstituted bonds that elongates the ring along the para-substituted axis). Without isotopic substitution, we cannot determine the relative contributions of the two ethylenic and three quinoidal (for DADSB) stretches to each mode. We believe that the lines near 1588 cm^{-1} (in DADSB) and 1575 cm^{-1} (in the dimers) carry most of the ethylenic stretching character because these modes show the greatest relative enhancement when excited in the longest-wavelength absorption band, but the DFT calculation places the ethylenic stretches higher in frequency than the ring-localized modes.

Modeling of the Resonance Raman Excitation Profiles and Absorption Spectra. Figure 8 compares the absorption spectrum of DADSB with the resonance Raman cross sections summed over all Raman lines. The Raman intensities track the absorption spectrum very closely for excitation wavelengths to the red of the first maximum, fall slightly below the absorption curve at the two bluer wavelengths within the main band (440 and 419 nm), and are much lower at excitation wavelengths within the second band (363 nm). The corresponding plots for dimers **5** and **6** are quite similar. For comparison, the calculated profiles for resonance with a *single* electronic transition peak slightly to the blue of the absorption maximum.

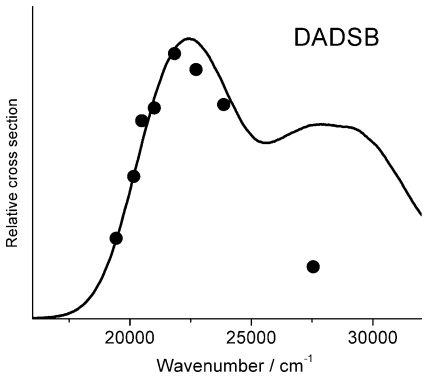

Figure 8. Resonance Raman cross section summed over all Raman lines (points) and absorption spectrum (curve) of DADSB in $CHCl_3$. The absorption and Raman cross sections have been scaled arbitrarily.

The absorption spectra and resonance Raman excitation profiles of the three chromophores were simulated by parametrizing a harmonic model for the ground- and excited-state potential energy surfaces and electronic spectral broadening. Some weak modes were omitted from the simulations, and lines that were too close in frequency to be separated reliably were grouped into a single vibration having an average frequency. Although we are interested mainly in the transition responsible for the longest-wavelength absorption band, there is enough spectral overlap with the fairly strong higher-energy band that more than one excited state must be included in the simulations. The higher-energy band was treated as a single transition. The Raman spectra at wavelengths to the red of the absorption maximum obtain most of their intensity from the lowest-energy transition, but at shorter wavelengths both transitions contribute, and they can interfere either constructively or destructively in the region of overlap.[35,45] This interference presumably accounts for the attenuation of the Raman profiles relative to the absorption curve at excitation wavelengths to the blue of the absorption maximum. We made the physically reasonable assumption that the excited-state displacements have the same sign in both electronic transitions and also assumed that both transitions have the same polarization direction. These choices maximize the destructive interference between the Raman amplitudes from the two states in the overlap region and produce the best fits to the excitation profiles.

TABLE 3: Absorption and Raman Spectral Modeling Parameters[a]

DADSB			dimer **5**			dimer **6**		
freq./cm^{-1}	Δ_1	Δ_2	freq./cm^{-1}	Δ_1	Δ_2	freq./cm^{-1}	Δ_1	Δ_2
962	0.20	0.3	605	0.29	0.29	603	0.29	0.29
1108	0.21	0.37	962	0.30	0.30	953	0.29	0.29
1175	0.47	0.58	999	0.24	0.24	997	0.25	0.25
1338	0.56	1.16	1109	0.32	0.32	1109	0.32	0.41
1414	0.21	0.28	1185	0.53	0.68	1183	0.57	0.87
1585	0.68	0.81	1257	0.43	0.50	1258	0.45	0.68
1626	0.30	0.41	1341	0.88	1.02	1339	0.88	1.36
			1412	0.22	0.24	1412	0.19	0.19
			1573	0.94	1.02	1570	0.92	1.11
			1620	0.33	0.43	1621	0.31	0.39
inhomog. width = 1400 cm^{-1}			inhomog. width = 900 cm^{-1}			inhomog. width = 960 cm^{-1}		
zero−zero energy = 20450 cm^{-1}			zero−zero energy = 17280 cm^{-1}			zero−zero energy = 17250 cm^{-1}		
(state 1), 21080 cm^{-1} (state 2)			(state 1), 18930 cm^{-1} (state 2)			(state 1), 18600 cm^{-1} (state 2)		
solvent reorg. energy = 1040 cm^{-1}			solvent reorg. energy = 1890 cm^{-1}			solvent reorg. energy = 2160 cm^{-1}		
(state 1), 5520 cm^{-1} (state 2)			(state 1), 6340 cm^{-1} (state 2)			(state 1), 6340 cm^{-1} (state 2)		
transition length = 2.79 Å			transition length = 3.25 Å			transition length = 3.24 Å		
(state 1), 2.50 Å (state 2)			(state 1), 2.71 Å (state 2)			(state 1), 2.50 Å (state 2)		

[a] Excited-state and ground-state frequencies were assumed equal. Δ_n is the displacement between the potential minima of the ground state and the nth excited state in dimensionless normal coordinates.

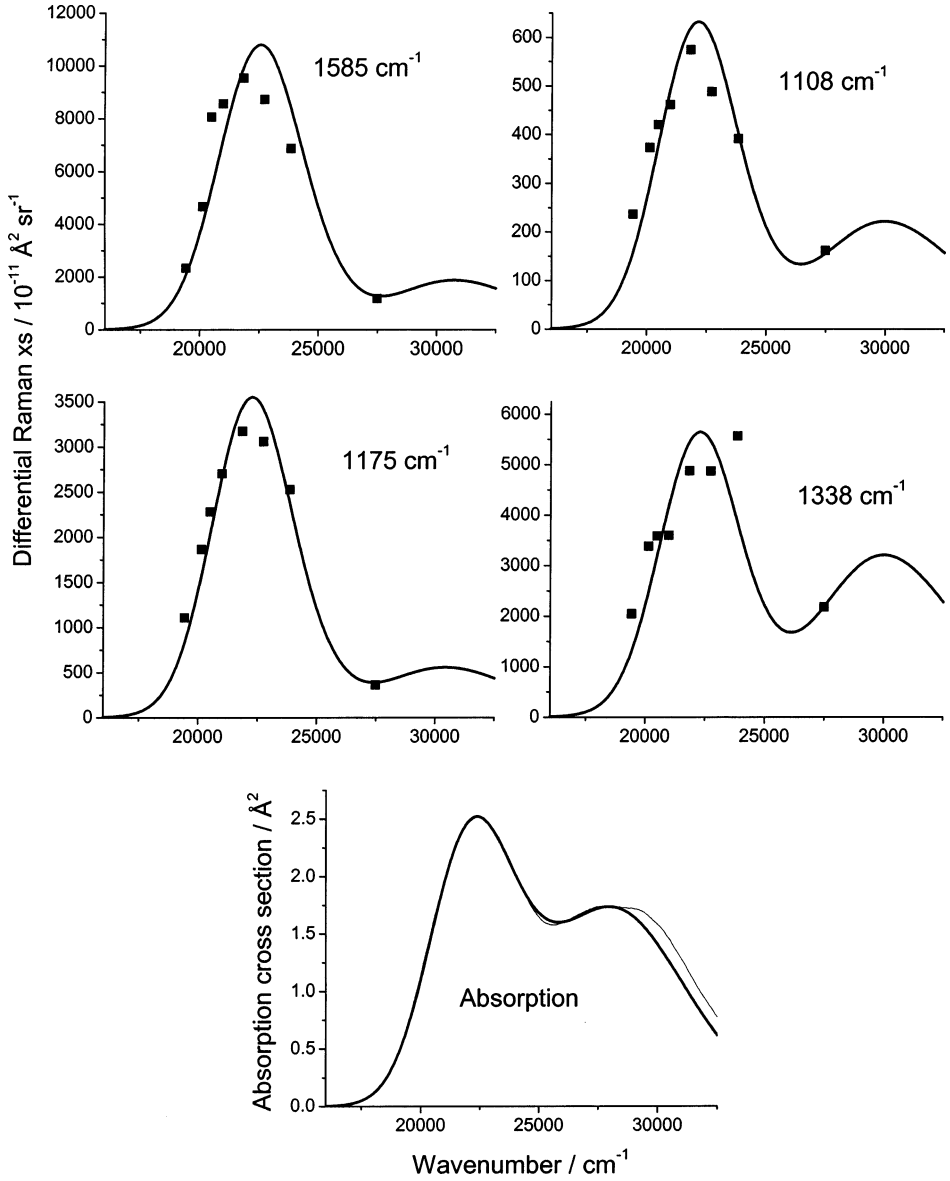

Figure 9. Experimental (points and thin line) and calculated (thick line) absorption spectrum and selected resonance Raman excitation profiles for DADSB in $CHCl_3$. Calculations use the parameters of Table 3.

Table 3 gives the best-fit modeling parameters for all three molecules, and Figure 9 shows calculated fits to the absorption spectrum and the excitation profiles for several modes of DADSB. The calculated profiles reproduce the observed narrowing on the blue side relative to the absorption spectrum. There is considerable uncertainty in the modeling parameters because of the substantial interference between the two transitions in the Raman amplitude and the likelihood, based on the breadth of the second band, that it actually contains more than one transition. The parameters for the second state cannot be considered very meaningful, as we have only one excitation wavelength in resonance with this state. However, comparison of the model parameters for the first transition generates a few useful insights. Although **5** and **6** have slightly greater oscillator strengths for the lowest-energy band, the monomer has somewhat higher Raman cross-sections based on either a mode-by-mode comparison or summed over all Raman fundamentals. This implies that the dimers have smaller displacements and/or a greater degree of homogeneous broadening (larger solvent reorganization energy) than the monomer; our modeling results suggest that the latter factor dominates, and that the dimers actually have somewhat larger displacements than the monomer. The close similarity of the parameters for the two dimers is consistent with their similar spectroscopy.

Discussion

Comparison of the absorption spectra of **5** and **6** (Figure 2) with predictions of the excitonically coupled dimer model immediately reveals the inadequacy of that model for describing the spectroscopy of these molecules. That model would describe these dimers as identical (in the absence of an environment) monomers with their molecular planes parallel and separated by a distance R. In this geometry, the interaction energy is given by $V = \mu^2 \cos\phi/R^3$ where μ is the transition dipole moment and ϕ is the angle between transition dipoles.[46] The true excited states are $\Psi_\pm = (1/\sqrt{2})(\psi_A \pm \psi_B)$ where ψ_A and ψ_B are the states that have the excitation localized on one monomer. The transition frequencies to these two states are $\nu_\pm = \nu_0 \pm V$ where ν_0 is the transition frequency of the monomer, and their oscillator strengths are $f_\pm = f_0(1 \pm \cos\phi)$ where f_0 is the monomer's oscillator strength.[47] The angle ϕ is estimated from the DFT STO-3G geometries as 130° for **6** and 50° for **5**. For dimer **6**, V is negative, making Ψ_- the more strongly allowed state and also the higher-energy one; for **5**, V is positive, making Ψ_+ the stronger transition and also the higher-energy one. Thus, the simple excitonic coupling model would predict that both **5** and **6** have their longest-wavelength transitions blue-shifted relative to the monomer (H-dimers), but in fact, both are red-shifted. Furthermore, the blue-shift should be enormous; for a monomer transition dipole length of 2.79 Å and an intermolecular separation of ∼3.3 Å, the coupling strength is calculated to be about 16 000 cm^{-1}. Finally, the total oscillator strength for the dimer (sum of both transitions) should theoretically be twice that of the monomer, contrary to observation.

The excitonic coupling model as applied above is clearly oversimplified and can be improved by introducing a number of refinements. For example, more sophisticated treatments of the interaction between molecular charge distributions[1,48−50] generally reduce the calculated coupling strength from that obtained in the point-dipole limit. Allowing the two monomers to have slightly nondegenerate electronic transitions because of inequivalent solvation will also modify the calculated transition energies and oscillator strengths.[2,49,51−54] The electrostatic interaction between the permanent ground- and excited-state charge distributions of the two monomers will shift the electronic transitions through a pure solvent effect quite apart from any excitonic coupling.[55,56] Finally, coupling between multiple electronic transitions on each monomer will also modify the energies of the dimer transitions. None of these modifications seem likely to solve the qualitative problems with the model noted above, particularly the nonconservation of the oscillator strength. We performed ZINDO calculations on a noncovalent model for dimer **5** formed by taking two DADSB monomers in the calculated DFT 6-31G geometry, rotating the chains by 50°, and stacking them with their molecular planes varying distances apart. The total oscillator strength for the two lowest-energy allowed transitions is essentially constant for intermolecular separations of 4 Å or greater, and is reduced to 80% of this value at 3.1 Å, the approximate inter-ring separation in **5**. These results suggest that the reduction in oscillator strength between two monomers and the dimer is attributable at least in part to a breakdown of the exciton model, although it probably also has contributions from distortions of the monomer's geometry in the dimers. It appears that the dimers must be considered as completely new molecules having fundamentally different electronic states from those of the monomer. This conclusion is consistent with other experimental and theoretical results on these and related paracyclophane-linked dimers,[17,22,25] which indicate that electron transfer from one chain to the other through the paracyclophane moiety is reasonably facile.

The fluorescence anisotropies of the dimers differ considerably from the single-electronic-state value of 0.4, indicating that the long-wavelength absorption band of the dimers is composed of more than one electronic transition having nonzero oscillator strengths and differently oriented transition dipoles. In the simplest situation where one transition absorbs and a different one emits, the fluorescence anisotropy, assuming the molecule as a whole does not rotate during the time between absorption and emission, is given by

$$r = \frac{1}{5}(3\cos^2\theta - 1) \tag{2}$$

where θ is the angle between the two transition dipoles. The measured anisotropies for **5** and **6** of ∼0.2−0.3 correspond to average angles of ∼20−35°. In contrast, the resonance Raman depolarization ratio of $\rho = 0.33$ for all modes corresponds to an anisotropy of $r = 0.4$ and suggests that all three molecules have a single allowed electronic transition in this region. If, for example, there are two contributing electronic states having an angle θ between their transition moments, then the resonance Raman depolarization ratio for any particular vibrational transition is given by[36]

$$\rho(\omega,\theta) = \frac{1}{3}\frac{|\alpha_1(\omega)|^2 + |\alpha_2(\omega)|^2 + \left(\cos^2\theta - \frac{1}{2}\sin^2\theta\right)[\alpha_1^*(\omega)\alpha_2(\omega) + \alpha_1(\omega)\alpha_2^*(\omega)]}{|\alpha_1(\omega)|^2 + |\alpha_2(\omega)|^2 + \left(1 - \frac{2}{3}\sin^2\theta\right)[\alpha_1^*(\omega)\alpha_2(\omega) + \alpha_1(\omega)\alpha_2^*(\omega)]} \tag{3}$$

where $\alpha_1(\omega)$ and $\alpha_2(\omega)$ are the wavelength-dependent contributions to the Raman polarizability associated with the two electronic states. As long as both α_1 and α_2 are nonzero and θ is different from zero, the depolarization ratio should be different from 1/3. The difference between Raman and fluorescence polarizations suggests that while most of the oscillator strength in the first absorption band of the dimers is carried by a single transition or by multiple transitions having nearly the same

polarization direction, a lower-energy, differently polarized transition contributes to the emission.

This hypothesis appears consistent with the ZINDO calculations on both dimers at the DFT geometries, which predict a strong *x*-polarized transition 20−40 nm to the blue of a much weaker (∼8% the oscillator strength) *y*-polarized one (see Table 1). However, there is a problem with this analysis: The stronger transition must dominate the absorption at most excitation wavelengths, yet the fluorescence anisotropy is much closer to 0.4 (parallel absorbing and emitting dipoles) than to −0.2 (perpendicular dipoles). One possibility is that relaxation between the two excited states is slow enough that the higher-energy state does much of the emitting. This would be highly unusual; important violations of Kasha's Rule in large, solvated organic molecules are rarely encountered except in special cases such as azulene, where the energy gap between the lowest excited states is very large. Emission from higher excited states may be observed when the two states are sufficiently close in energy that both are populated at thermal equilibrium. We cannot discount this as a plausible explanation for our results, although for both dimers to have very similar and small (few hundred cm^{-1}) energy gaps would seem a bit fortuitous.

A more attractive possibility is that the angle between absorbing and emitting transition dipoles is actually much smaller than 90°. This is not possible in a static structure having true C_2 symmetry as indicated by Figure 1, but in any condensed-phase environment, the symmetry will be broken by transiently nonequivalent solvation of the two chains.[57,58] As geometric relaxation and solvent reorganization proceed, an excitation that was initially delocalized over both DADSB chains may become trapped on a single chain. The angle between the transition dipole of a single DADSB chain and the dipole for the strongly allowed transition of the delocalized system should be about 25°, in good agreement with the above experimental estimate of the angle between absorbing and emitting dipoles. Similar models incorporating static disorder (environmentally induced breaking of the degeneracy between nominally identical monomers), dynamic disorder (thermal excitation of vibrations), and dissipation (energy transfer from chromophores to environment) have been shown to account for rapid depolarization of the fluorescence in systems of coupled chromophores such as distyrylbenzene dendrimers[59] and the light-harvesting chlorophyll complexes of purple bacteria.[54,60,61] In our dimers, the "$t = 0$" emission (Raman scattering) arises from the same delocalized state that does the absorbing and exhibits the expected anisotropy for parallel absorbing and emitting dipoles. The time-integrated fluorescence involves mainly emission from a single chain on which the excitation has become trapped, and exhibits the expected anisotropy for absorbing and emitting dipoles at an angle of ∼25°. In the monomer, there is no such evolution from delocalized to localized excitation and the fluorescence retains nearly the same anisotropy as the resonance Raman. The slight depolarization of the monomer fluorescence probably reflects a small degree of librational freedom for the chromophore in its cavity in the polymer at room temperature. The close similarity of the monomer and dimer fluorescence band shapes (Figure 2) further supports this hypothesis, at least in the polymer films.

Resonance Raman intensity analysis of these molecules is somewhat compromised by the complexity of their absorption spectra. Although the Raman spectra excited on resonance with the two absorption bands are quite different, the calculated cross sections in both bands depend on the parameters for both states. This makes unique determination of the excited-state geometry changes and solvent reorganization energy difficult even for the lowest-energy transition, particularly since the higher-energy band probably contains more than one electronic transition. The best-fit simulation parameters for the lower-energy transition are only partly consistent with our prior expectations. The reduced zero−zero energies of both dimers relative to the monomer are an expected result of increased electronic delocalization, but the greater total vibrational reorganization energy in the dimers (∼1800 cm^{-1} vs 850 cm^{-1}) is not; internal reorganization energies generally decrease with increasing conjugation length. The greater solvent reorganization energy in the dimers compared with the monomer might be an expected result of a greater degree of charge separation in the vertically excited state of the more extended systems, but we might expect a large difference between the two dimers because of the difference in relative orientations of the electron donating and accepting groups; **5** has a much larger ground-state dipole moment than **6**[25] and should have a correspondingly larger dipole moment change upon electronic excitation. In fact, we find only subtle differences between dimers **5** and **6** in any of the spectroscopic observables we have examined.

Conclusions

The experimental and computational studies reported here are consistent with other recent studies which conclude that *noncovalent* "face-to-face" dimers of π-conjugated molecules cannot be adequately described by exciton coupling theory when the interchain distance is less than about 4 Å[50,62] and with other studies of paracyclophane-linked covalent dimers that indicate the importance of charge transfer between the chains.[22,25] Perhaps the most interesting result of the present work is the substantial depolarization of the time-integrated fluorescence from immobilized dimers relative to the prompt component of the emission (resonance Raman scattering). This difference is not observed in the monomer and indicates a change in the nature of the emitting state over the excited-state lifetime. Localization of an initially delocalized excitation on a single chain as the excited chromophore and surrounding polymer undergo geometric relaxation is suggested as one plausible mechanism consistent with the magnitude of the depolarization.

Acknowledgment. This work was supported by NSF Grants #CHE-0109920 to Kansas State University and #CHE-0342816 to the University of California, Merced. We thank Professor David F. Kelley for the use of his fluorometer and Dr. Nina Verdal for help in preparing the samples in polymer films.

References and Notes

(1) Krueger, B. P.; Scholes, G. D.; Fleming, G. R. *J. Phys. Chem. B* **1998**, *102*, 5378−5386.

(2) Freiberg, A.; Timpmann, K.; Ruus, R.; Woodbury, N. W. *J. Phys. Chem. B* **1999**, *103*, 10032−10041.

(3) Nguyen, T.-Q.; Martini, I. B.; Liu, J.; Schwartz, B. J. *J. Phys. Chem. B* **2000**, *104*, 237−255.

(4) Deans, R.; Kim, J.; Machacek, M. R.; Swager, T. M. *J. Am. Chem. Soc.* **2000**, *122*, 8565−8566.

(5) Lemmer, U.; Heun, S.; Mahrt, R. F.; Scherf, U.; Hopmeier, M.; Siegner, U.; Göbel, E. O.; Müllen, K.; Bässler, H. *Chem. Phys. Lett.* **1995**, *240*, 373−378.

(6) Lim, S.-H.; Bjorklund, T. G.; Bardeen, C. J. *J. Phys. Chem. B* **2004**, *108*, 4289−4295.

(7) Yitzchaik, S.; Di Bella, S.; Lundquist, P. M.; Wong, G. K.; Marks, T. J. *J. Am. Chem. Soc.* **1997**, *119*, 2995−3002.

(8) Liakatas, I.; Cai, C.; Bösch, M.; Jäger, M.; Bosshard, C.; Günter, P.; Zhang, C.; Dalton, L. R. *Appl. Phys. Lett.* **2000**, *76*, 1368−1370.

(9) Le Duff, A.-C.; Canva, M.; Lévy, Y.; Brun, A.; Ricci, V.; Pliska, T.; Meier, J.; Stegeman, G. I.; Chaput, F.; Boilot, J.-P.; Toussaere, E. *J. Opt. Soc. Am. B* **2001**, *18*, 1827−1831.

(10) Harper, A. W.; Sun, S.; Dalton, L. R.; Garner, S. M.; Chen, A.; Kalluri, S.; Steier, W. H.; Robinson, B. H. *J. Opt. Soc. Am. B* **1998**, *15*, 329−337.
(11) Fulton, R. L.; Gouterman, M. *J. Chem. Phys.* **1964**, *41*, 2280−2286.
(12) Spano, F. C. *J. Chem. Phys.* **2001**, *114*, 5376−5390.
(13) Spano, F. C. *J. Chem. Phys.* **2003**, *118*, 981−994.
(14) Würthner, F.; Yao, S.; Debaerdemaeker, T.; Wortmann, R. *J. Am. Chem. Soc.* **2002**, *124*, 9431−9447.
(15) Song, X.; Geiger, C.; Leinhos, U.; Perlstein, J.; Whitten, D. G. *J. Am. Chem. Soc.* **1994**, *116*, 10340−10341.
(16) Chen, H.; Farahat, M. S.; Law, K.-Y.; Whitten, D. G. *J. Am. Chem. Soc.* **1996**, *118*, 2584−2594.
(17) Bazan, G. C.; Oldham, W. J., Jr.; Lachicotte, R. J.; Tretiak, S.; Chernyak, V.; Mukamel, S. *J. Am. Chem. Soc.* **1998**, *120*, 9188−9204.
(18) Oldham, W. J., Jr.; Miao, Y.-J.; Lachicotte, R. J.; Bazan, G. C. *J. Am. Chem. Soc.* **1998**, *120*, 419−420.
(19) Wang, S.; Bazan, G. C.; Tretiak, S.; Mukamel, S. *J. Am. Chem. Soc.* **2000**, *122*, 1289−1297.
(20) Bartholomew, G. P.; Bazan, G. C. *Acc. Chem. Res.* **2001**, *34*, 30−39.
(21) Verdal, N.; Godbout, J. T.; Perkins, T. L.; Bartholomew, G. P.; Bazan, G. C.; Kelley, A. M. *Chem. Phys. Lett.* **2000**, *320*, 95−103.
(22) Zyss, J.; Ledoux, I.; Volkov, S.; Chernyak, V.; Mukamel, S.; Bartholomew, G. P.; Bazan, G. C. *J. Am. Chem Soc.* **2000**, *122*, 11956−11962.
(23) Moran, A. M.; Bartholomew, G. P.; Bazan, G. C.; Kelley, A. M. *J. Phys. Chem. A* **2002**, *106*, 4928−4937.
(24) Bartholomew, G. P.; Bazan, G. C. *J. Am. Chem. Soc.* **2002**, *124*, 5183−5196.
(25) Bartholomew, G. P.; Ledoux, I.; Mukamel, S.; Bazan, G. C.; Zyss, J. *J. Am. Chem. Soc.* **2002**, *124*, 13480−13485.
(26) Myers, A. B. In *Laser Techniques in Chemistry*; Myers, A. B., Rizzo, T. R., Eds.; Wiley: New York, 1995; pp 325−384.
(27) Myers, A. B.; Li, B.; Ci, X. *J. Chem. Phys.* **1988**, *89*, 1876−1886.
(28) Shriver, D. F.; Dunn, J. B. R. *Appl. Spectrosc.* **1974**, *28*, 319−323.
(29) Moran, A. M.; Delbecque, C.; Kelley, A. M. *J. Phys. Chem. A* **2001**, *105*, 10208−10219.
(30) Foster, C. E.; Barham, B. P.; Reid, P. J. *J. Chem. Phys.* **2001**, *114*, 8492−8504.
(31) Verdal, N.; Kelley, A. M. *J. Chem. Phys.* **2002**, *117*, 8996−9008.
(32) Frisch, M. J.; Trucks, G. W.; Schlegel, H. B.; Scuseria, G. E.; Robb, M. A.; Cheeseman, J. R.; Zakrzewski, V. G.; Montgomery, J. A., Jr.; Stratmann, R. E.; Burant, J. C.; Dapprich, S.; Millam, J. M.; Daniels, A. D.; Kudin, K. N.; Strain, M. C.; Farkas, O.; Tomasi, J.; Barone, V.; Cossi, M.; Cammi, R.; Mennucci, B.; Pomelli, C.; Adamo, C.; Clifford, S.; Ochterski, J.; Petersson, G. A.; Ayala, P. Y.; Cui, Q.; Morokuma, K.; Malick, D. K.; Rabuck, A. D.; Raghavachari, K.; Foresman, J. B.; Cioslowski, J.; Ortiz, J. V.; Stefanov, B. B.; Liu, G.; Liashenko, A.; Piskorz, P.; Komaromi, I.; Gomperts, R.; Martin, R. L.; Fox, D. J.; Keith, T.; Al-Laham, M. A.; Peng, C. Y.; Nanayakkara, A.; Gonzalez, C.; Challacombe, M.; Gill, P. M. W.; Johnson, B. G.; Chen, W.; Wong, M. W.; Andres, J. L.; Head-Gordon, M.; Replogle, E. S.; Pople, J. A. *Gaussian 98*, revision A.7; Gaussian, Inc.: Pittsburgh, PA, 1998.
(33) Schaftenaar, G. Molden 3.6; CMBI: The Netherlands, 2000.
(34) Waterland, M. R.; Kelley, A. M. *J. Chem. Phys.* **2000**, *113*, 6760−6773.
(35) Egolf, D. S.; Waterland, M. R.; Kelley, A. M. *J. Phys. Chem. B* **2000**, *104*, 10727−10737.
(36) Lilichenko, M.; Tittelbach-Helmrich, D.; Verhoeven, J. W.; Gould, I. R.; Myers, A. B. *J. Chem. Phys.* **1998**, *109*, 10958−10969.
(37) Rhodes, T. A.; Farid, S.; Goodman, J. L.; Gould, I. R.; Young, R. H. *J. Am. Chem. Soc.* **1999**, *121*, 5340−5341.
(38) Bree, A.; Edelson, M. *Chem. Phys.* **1980**, *51*, 77−88.
(39) Edelson, M.; Bree, A. *Chem. Phys. Lett.* **1976**, *41*, 562−564.
(40) Mathies, R. A.; Smith, S. O.; Palings, I. In *Biological Applications of Raman Spectroscopy*; Spiro, T. G., Ed.; John Wiley & Sons: New York, 1987; Vol. 2, pp 59−108.
(41) Karabunarliev, S.; Baumgarten, M.; Bittner, E. R.; Müllen, K. *J. Chem. Phys.* **2000**, *113*, 11372−11381.
(42) Moran, A. M.; Kelley, A. M. *J. Chem. Phys.* **2001**, *115*, 912−924.
(43) Varsanyi, G. *Assignments for Vibrational Spectra of Seven Hundred Benzene Derivatives*; Wiley: New York, 1974.
(44) Kwok, W. M.; Ma, C.; Matousek, P.; Parker, A. W.; Phillips, D.; Toner, W. T.; Towrie, M.; Umapathy, S. *J. Phys. Chem. A* **2001**, *105*, 984−990.
(45) Markel, F.; Myers, A. B. *J. Chem. Phys.* **1993**, *98*, 21−30.
(46) Stone, A. J. *The Theory of Intermolecular Forces*; Oxford University Press: New York, 1996.
(47) Cantor, C. R.; Schimmel, P. R. *Biophysical Chemistry Part II: Techniques for the Study of Biological Structure and Function*; W. H. Freeman & Company: New York, 1980.
(48) Czikklely, V.; Forsterling, H. D.; Kuhn, H. *Chem. Phys. Lett.* **1970**, *6*, 207−210.
(49) Marguet, S.; Markovitsi, D.; Millié, P.; Sigal, H.; Kumar, S. *J. Phys. Chem. B* **1998**, *102*, 4697−4710.
(50) Beljonne, D.; Cornil, J.; Silbey, R.; Millié, P.; Brédas, J. L. *J. Chem. Phys.* **2000**, *112*, 4749−4758.
(51) Spano, F. C. *J. Chem. Phys.* **2002**, *116*, 5877−5891.
(52) van Oijen, A. M.; Ketelaars, M.; Köhler, J.; Aartsma, T. J.; Schmidt, J. *Biophys. J.* **2000**, *78*, 1570−1577.
(53) Wu, H.-M.; Ratsep, M.; Lee, I.-J.; Cogdell, R. J.; Small, G. J. *J. Phys. Chem. B* **1997**, *101*, 7654−7663.
(54) Kumble, R.; Hochstrasser, R. M. *J. Chem. Phys.* **1998**, *109*, 855−865.
(55) Kelley, A. M. *J. Chem. Phys.* **2003**, *119*, 3320−3331.
(56) Painelli, A.; Terenziani, F. *Synth. Met.* **2003**, *139*, 779−781.
(57) Johnson, A. E.; Myers, A. B. *J. Phys. Chem.* **1996**, *100*, 7778−7788.
(58) Waterland, M. R.; Stockwell, D.; Kelley, A. M. *J. Chem. Phys.* **2001**, *114*, 6249−6258.
(59) Varnavski, O.; Samuel, I. D. W.; Palsson, L.-O.; Beavington, R.; Burn, P. L.; Goodson, T., III. *J. Chem. Phys.* **2002**, *116*, 8893−8903.
(60) Kühn, O.; Sundström, V.; Pullerits, T. *Chem. Phys.* **2002**, *275*, 15−30.
(61) Kleinekathöfer, U.; Barvik, I.; Herman, P.; Kondov, I.; Schreiber, M. *J. Phys. Chem. B* **2003**, *107*, 14094−14102.
(62) Leng, W.; Würthner, F.; Kelley, A. M. *J. Phys. Chem. B* **2004**, *108*, 10284−10294.